This is a PDF file of an unedited manuscript that has been accepted for publication. Final edited form is published in *Langmuir, 2014, 30:15451−15461*. http://dx.doi.org/10.1021/la5038102

Mechanism of in-situ surface polymerization of gallic acid in an environmental-inspired preparation of carboxylated core-shell magnetite nanoparticles

Ildikó Y. Tóth[1], Márta Szekeres[1], Rodica Turcu[2], Szilárd Sáringer[1], Erzsébet Illés[1], Dániel Nesztor[1], Etelka Tombácz[1*]*

[1]Department of Physical Chemistry and Materials Science, University of Szeged, Aradi vt 1, 6720 Szeged, Hungary

[2]National Institute R&D for Isotopic and Molecular Technology, Cluj-Napoca 400293, Romania

Corresponding authors

M. Szekeres (szekeres@chem.u-szeged.hu) and E. Tombácz (tombacz@chem.u-szeged.hu)

Graphical abstract

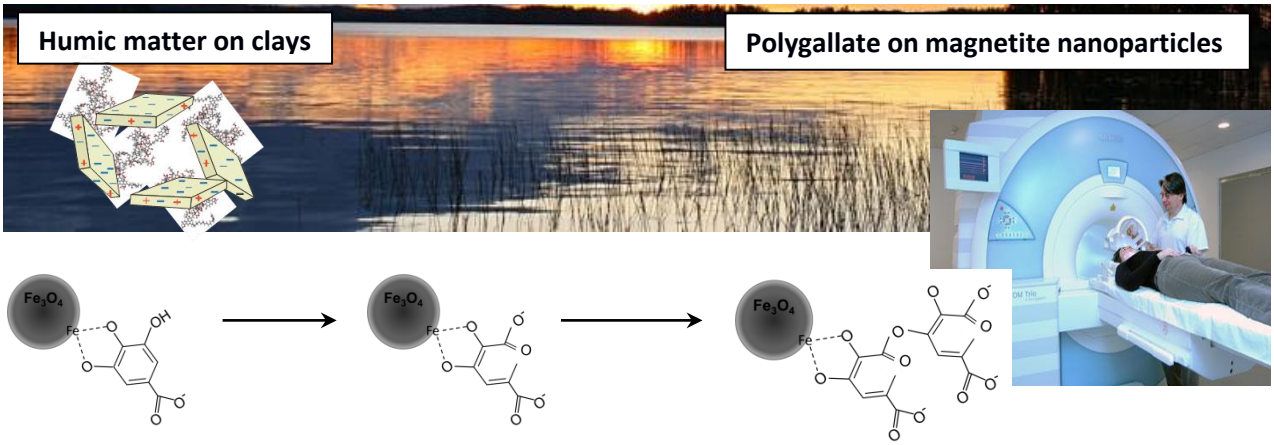

Abstract

Magnetite nanoparticles (MNPs) with biocompatible coatings are good candidates for MRI (magnetic resonance imaging) contrasting, magnetic hyperthermia treatments and drug delivery systems. The spontaneous surface induced polymerization of dissolved organic matter on environmental mineral particles inspired us to prepare carboxylated core-shell MNPs by using a ubiquitous polyphenolic precursor. Through the adsorption and in-situ surface polymerization of gallic acid (GA), a polygallate (PGA) coating is formed on the nanoparticles (PGA@MNP) with possible antioxidant capacity. The

present work explores the mechanism of polymerization with the help of potentiometric acid-base titration, dynamic light scattering (for particle size and zeta potential determination), UV-Vis (UV-visible light spectroscopy), FTIR-ATR (Fourier-transformed infrared spectroscopy by attenuated total reflection) and XPS (X-ray photoelectron spectroscopy) techniques. We observed the formation of ester and ether linkages between gallate monomers both in solution and in the adsorbed state. Higher polymers were formed in the course of several weeks both on the surface of nanoparticles and in the dispersion medium. The ratio of the absorbances of PGA supernatants at 400 and 600 nm (i.e., the E4/E6 ratio commonly used to characterize the degree of polymerization of humic materials) was determined to be 4.3, similar to that of humic acids. Combined XPS, dynamic light scattering and FTIR-ATR results revealed that prior to polymerization, the GA monomers became oxidized to polycarboxylic acids due to ring opening while Fe^{3+} ions reduced to Fe^{2+}. Our published results on the colloidal and chemical stability of PGA@MNPs are referenced thoroughly in the present work. Detailed studies on biocompatibility, antioxidant property and biomedical applicability of the particles will be published.

Keywords

biocompatible coating, core-shell nanoparticles, magnetic nanoparticles, polygallic acid, surface induced polymerization, X-ray photoelectron spectroscopy

1. Introduction

Many different types of core-shell magnetic iron oxide (magnetite) nanoparticles (MNPs) have already been designed for medical applications such as magnetic imaging (MRI – magnetic resonance imaging and MPI – magnetic particle imaging), local heating (magnetic hyperthermia), or targeted drug delivery. All these theranostic tools aim to exploit the great potential in controlling the motion of nanoparticles by an external magnetic field.[1-6] The coating shell is expected to provide necessary colloidal stability under physiological conditions and to serve as a location for anchoring active agents to the particles.

Both of the commonly applied strategies of coating nanoparticles with polymer or polyelectrolyte shells – chemical synthesis and physico-chemical processes like adsorption – have their advantages and drawbacks. Advanced organic chemistry for covalent attachment often requires synthesis conditions that are not compatible with biological media (e.g., toxic monomers, by-products or organic solvents, which are difficult to remove from the products). Colloidal stability and salt tolerance tests of nanoparticles with chemically grafted shells are very rarely presented in the literature and so their eligibility for biomedical applications is still lacking physico-chemical approval. Dufort and co-authors[7] suggested undertaking a specific series of physico-chemical and in-vivo/in-vitro biological tests prior to clinical trials and Szekeres and co-authors[8] proposed a detailed protocol for the physico-chemical testing procedure. The latter protocol comprises a sequence of tests to probe the chemical and colloidal stability and salt tolerance of coated nanoparticles. The strategy of nanoparticle coating via adsorption of polymers or polyelectrolytes is fully biocompatible. The adsorption forces, however, can be too weak for a sufficiently durable core-shell structure. On the other hand, too strong affinity of solute to the metal ions of the crystal lattice could induce the dissolution of nanoparticles. A representative example of the latter is the enhanced dissolution of iron from citrate-coated iron oxide nanoparticles.[8-11] The adsorption interactions must be optimized by selecting adequate coating molecules and by carefully adjusting the solution conditions so that the resulting shells compete in strength and functionality with those produced in surface chemical reactions.

A novel approach to the synthesis of core-shell nanoparticles would be the environmental-inspired production of coatings via the adsorption of monomers with subsequent in-situ surface polymerization mimicking the process of humic adic formation from dissolved organic matter on the surface of clay particles in nature. It combines the advantages of physico-chemical surface modification and chemical binding in that i) the procedure is all-natural with no toxic constituents and ii) the coating can be removed only by chemical reactions. We have chosen gallic acid (GA) as monomer for the preparation of polygallate shell on MNPs (PGA@MNP) since GA possesses the main characteristics of dissolved organic matter necessary for spontaneous formation of organic coating: the presence of phenolic and carboxylic moieties and an aromatic ring in its structure. We have discussed the formation procedure

and the durability of the coating shell, the chemical and colloidal stability of the PGA@MNPs and their salt tolerance as well in earlier publications.[8,12,13] The present paper is mainly devoted to exploring the mechanism of surface induced polymerization of GA on iron oxide nanoparticles.

Many GA-like compounds (phenolic acids) are present in large concentrations in different plants.[14] GA is frequently used as a model for food polyphenols[15] and the concentration of dietary polyphenols is often expressed in gallic acid equivalents. GA-like compounds are also used for metal ion removal in biomedicine[16] and in water and wastewater treatment[17-20] due to their capability to chelate toxic heavy metal and transition metal ions, and radioactive traces.

Gallic acid (GA) can easily bind to the surface Fe^{3+} ions of magnetite nanoparticles via bidentate chelate formation through the two phenolic OH groups in ortho position (catechol group)[12,13] similarly to the GA chelation of surface Ti^{4+} ions of TiO_2 particles.[22] It has also been established that clay minerals and some oxides can catalyze the polymerization of catechol-type organic molecules leading to the formation of humic acids and humic like compounds.[23] In the environment, humic coating is formed spontaneously on mineral particles (clays, oxides) from the random fragments of biomolecules like degradation products of lignin, carbohydrates and proteins or polyphenols and aromatic polyacids. Wang and co-authors[24-27] have shown that the abiotic synthesis of fulvic and humic acids on the surface of clay minerals can proceed through heterogeneous catalysis (autooxidation and surface polymerization) of polyacids, gallic acid among them. Tombácz and coworkers synthesized fulvic acid on montmorillonite by heterogeneous catalysis of gallic acid with average molecular weight of 840 g/mol as determined by vapor pressure osmometry.[28]

Overall, our synthesis of core-shell PGA@MNPs for bio-application was inspired by the environmental process of surface induced polymerization of small organic acids possessing OH moieties. Based on the analogy to humic formation in the environment, the spontaneous formation of a polygallate (PGA) shell on the MNP cores is in fact a chemical transformation under mild conditions and it should result in a persistent coating. The PGA@MNPs are expected to be sufficiently stable in biological media similarly to the recalcitrant humic acids existing in a biogeochemical metastable state in nature.

We have shown in a series of previous publications[8,12,13] that surface polymerized gallic acid protects the MNPs from aggregation at physiological pH and salt concentration and ensures colloidal and chemical stability necessary for biomedical applications. In the present work, we examine the mechanism of GA adsorption and surface polymerization in detail by using potentiometric acid-base titration, dynamic light scattering, UV-Vis, FTIR-ATR and X-ray photoelectron spectroscopy (XPS) methods. Our studies on the biocompatibility and biomedical performance of the PGA@MNPs will be published subsequently.

2. Materials and methods

2.1 Materials. Magnetite (Fe_3O_4) nanoparticles were synthesized by alkaline hydrolysis of iron(II) and iron(III) salts.[29-31] Concentrated iron salt solutions ($FeCl_2 \cdot 4H_2O$ and $FeCl_3 \cdot 6H_2O$, Molar, Hungary) were mixed at the ratio of iron(II) to iron(III) 1:2 and filtered into fresh ultrapure water using a microfilter (0.2 μm). Freshly prepared NaOH solution was added to the iron salt solution under rigorous stirring. The first half of the volume was added slowly and the remaining all at once. The NaOH was added in 10 % excess related to the hydrolysis equivalent. The resulting black suspension was stirred for several minutes and then transferred into a large volume of ultrapure water. The suspension was washed with water several times, acidified with HCl solution to pH~2, and washed again with water until peptization occurred. Finally, the sample was dialyzed against a 0.001 M HCl solution. The magnetite concentration was determined gravimetrically. The stock suspension was stored in the dark at 4 °C. The product was identified by X-ray diffraction (Philips PW 1830/PW 1820 X-ray diffractometer operating in the reflection mode with CuK_α radiation) as magnetite. The pH-dependent surface charge density was characterized quantitatively in potentiometric acid–base titration experiments.[31] The pH of PZC (point of zero charge) of the synthesized magnetite is 7.9 ±0.1.

Analytical grade gallic acid obtained from Carlo Erba was used throughout the experiments. To set the ionic strength and pH of the samples, NaCl, NaOH and HCl (Molar, Hungary, analytical grade) solutions were used. Ultrapure water (18 MΩ) from a HumanCorp Zeneer water purification system was used in the experiments. The experiments were performed at room temperature, if not stated otherwise.

2.2 Potentiometric acid-base titration. Gallic acid solution of 2.4 mmol/dm^3 concentration was prepared in a NaCl background electrolyte to provide constant ionic strength by using CO_2-free ultrapure water. Carbonate-free base titrant was prepared after rinsing NaOH grains three times with CO_2-free purified water. The NaOH solution was standardized using benzoic acid (analytical grade, Molar), and it was applied right away to standardize the acid titrant (HCl solution). Secondary standard buffer solutions of Radelkis Ltd. (Hungary) of pH (25 ^{0}C)=2.07±0.03 (RK-21), pH (25 ^{o}C)=7.10±0.03 (RK-71) and pH(25 ^{o}C)=9.31±0.03 (RK-91) were used for buffer calibrations. The titrations were carried out under programmed stirring and N_2 bubbling (nitrogen 4.5 from Messer, min. 99.995% purity with 10 ppm O_2 and no CO_2 content). A gas-washing bottle filled with CO_2 free ultrapure water was used to wet the N_2 gas flow. The automatic titration setup comprises a sample holder, a magnetic stirrer, N_2 gas inlet, acid and base burettes (Metrohm, Dosimat 665), a combined pH glass electrode (OP-0808P of Radelkis Ltd., Hungary) and a high precision potentiometer with pH preamplifier. The accuracy of mV readings of the potentiometer is ±0.01 mV. Homemade software (Gimet-1) was used to control the titration process. The temperature was held constant (25 ± 0.5 ^{o}C). The combined target uncertainty involved in the titration and calculation procedures is estimated as ±0.1 pH units. The main contributors are the uncertainties in buffer solution pH, electrode mV readings and volume errors in the solution preparations and dosing of titrant. The complete titration experiment and data evaluation procedure is discussed in our previous publication.[32] The whole cycle consisting of one up (pH increasing from 3 to 11) and one down (pH decreasing from 11 to 3) titration was repeated three times and the representative curves were used to define dissociation constants via derivation and using the program FITEQL 4.0.

2.3 GA adsorption and desorption on MNPs. The adsorption isotherms of GA at pH~6.5 and NaCl concentration of 0.01 M were determined by the batch method. The magnetite suspensions (10 g/L) were equilibrated with a series of GA solutions (0 –10 mmol/L) in closed test tubes for a period between 24 h and five weeks at room temperature. By adding small portions of a NaOH or HCl solution, the pH was adjusted to 6.5 ± 0.1 and checked again at the end of adsorption. After perfectly separating the solid particles by centrifugation (13000 rpm for 1 h), the equilibrium concentrations were determined at the

end of the equilibration periods (24 h, 1, 2 and 5 weeks) by measuring the absorbance of supernatants at 260 nm in an USB4000 spectrometer (Ocean Optics, USA). At higher GA concentrations the separation was assisted by a permanent magnet and membrane filtration (0.22 μm MILLEX-GP). Three parallel experiments were measured for reproducibility. During standstill for weeks at room temperature, the spontaneous formation of polygallate was allowed to take place in the adsorption samples, which became perceivable after longer period. Samples with different GA loading were prepared and the PGA coating and PGA@MNPs were characterized. The size of the magnetic core was checked before and after the in situ surface polymerization of GA by means of transmission electron microscopy (TEM) by using a Philips CM-10 apparatus supplied with a Megaview-II camera (Amsterdam, Netherlands).

Desorption isotherms were determined using the same procedure as that in the adsorption experiments. After establishing the adsorption equilibrium, the dispersions were doubly diluted and a period of 24 h was allowed for GA desorption.

2.4 Dynamic light scattering measurements. The hydrodynamic diameter of the particles was measured in a NanoZS apparatus (Malvern, UK) with a He-Ne laser (λ = 633 nm), operating in backscattering mode at an angle of 173°. The stock sols of magnetite particles were diluted with a NaCl electrolyte (10 mM) to 0.1 g/L solid content. The ionic strength was constant and pH was adjusted in the range of 3 to 11, directly before the measurements. Before the measurements, the samples were homogenized by ultrasound agitation for 10 s and allowed to relax for 110 s. The average value of the hydrodynamic diameter (Z_{ave}) was calculated from the 3rd order cumulant fit of the correlation function. The values of standard deviation of Z_{ave} varied between 15 (for the primary particles) and 150 (for aggregates) nm.

In the experiments on kinetics of coagulation, we measured the increase in the hydrodynamic diameter of GA- and PGA-coated MNPs with time by using a Nano ZS apparatus (Malvern). The measurements were performed at pH~6.5 with increasing amount of added electrolyte NaCl. The dispersions were aged for one day (GA@MNPs) or five weeks (PGA@MNPs). The data were collected for every minute in the course of 15 min. The stability ratio W was determined as the ratio of the slopes of the kinetic curves

measured in the linear region of aggregation (dimer formation) above the critical coagulation concentration (CCC) of the electrolyte (fast coagulation) and at moderate electrolyte concentrations (slow coagulation). The change in the stability ratio (log W) as a function of the electrolyte concentration (log c_{NaCl}) was used to determine CCC, which characterizes the salt tolerance of the MNP dispersions. The experiments were repeated three times and the deviations in the log W values varied from ±0.1 to ±0.2, higher for the larger Z_{ave} values.

2.5 Electrokinetic potential measurements. The changes in the electrophoretic mobility of GA@MNPs (dispersed in a 10 mM NaCl medium) in the function of pH and GA addition were measured by using a Nano ZS apparatus (Malvern). Disposable zeta cells (DTS 1060) were used in the experiments. The Smoluchowski equation was applied to convert the electrophoretic mobilities to electrokinetic potential (i.e., zeta potential) values. The instrument was calibrated by measuring the zeta potential of a zeta-standard (55 ± 5 mV) supplied by Malvern and the accuracy of the measurements is ±5 mV as given by Malvern. The concentration of the dispersions was set to give an optimal intensity of ~105 counts per second. Prior to the measurements, the samples were agitated with ultrasound for 10 s and allowed to relax for 2 min.

2.6 UV-Vis, FTIR-ATR and XPS measurements. UV-Vis spectra of GA and PGA solutions (without MNP addition or as supernatants of the adsorption series) were recorded in the 200–800 nm wavelength range using a USB4000 spectrometer (Ocean Optics, USA). The concentration of GA in solutions without the MNPs was 12 mmol/dm^3 and if necessary, diluted for UV-Vis measurements.

FTIR-ATR spectra were recorded with a Bio-Rad Digilab Division FTS-65A/896 spectrometer (with DTGS detector), using a Harrick's Meridian Split Pea Diamond ATR accessory. The absorbance of the samples was measured in single reflection mode over the 400−4000 cm^{-1} range (with resolution of 2 cm^{-1}), accumulating 256 scans. Magnetite suspension, GA solution and GA@MNP or PGA@MNP suspensions (at pH~6.5 in 10 mM NaCl) were dried on the crystal surface. The spectrum of MNP was

subtracted from those of GA@MNP and PGA@MNP. The amount of added GA was 5 mmol/g(MNP). The background spectra were measured on a clean and dry diamond crystal.

XPS spectra were recorded using an XPS spectrometer SPECS equipped with an Al/Mg dual-anode X-ray source, a PHOIBOS 150 2D CCD hemispherical energy analyzer and a multi-channeltron detector with vacuum maintained at 1 x 10^{-9} torr. The $Al_{K\alpha}$ X-ray source (1486.6 eV) was operated at 200 W. The XPS survey spectra were recorded at 30 eV pass energy, 0.5 eV/step. The high-resolution spectra for individual elements were recorded by accumulating 10 scans at 30 eV pass energy and 0.1 eV/step. PGA@MNPs of 1 mmol GA/g MNP concentration prepared at pH ~6.5 and 10 mM NaCl were aged for 4 weeks before the XPS experiments. The aqueous suspensions of nanoparticles were dried on an indium foil and the surface of the samples was cleaned by argon ion bombardment (300 V). The spectra were recorded before and after the cleaning. Data analysis and curve fitting was performed using CasaXPS software with a Gaussian-Lorentzian product function and a non-linear Shirley background subtraction. The high resolution spectra were deconvoluted into the components corresponding to particular bond types.

3. Results and discussion

3.1 Oligomerization of gallic acid in aqueous solutions

We measured the changes in the UV-Vis spectra of aqueous GA solutions in response to acid or base addition. Figure 1 shows the gradual color change of a 12 mmol/dm^3 GA solution at 10 mM ionic strength within 2 minutes after adding the amount of NaOH necessary to change the pH from ~4 to ~11 as calculated the from acid-base titration of GA. The color of the originally colorless solution is changing to orange and then to green. At high pH, the dissociation of ortho phenolic OH groups results in the formation of resonant structures[33] and the enhanced conjugation of the original polyphenol ring changes the color of the solution. Radical formation in the presence of oxygen[34,35] strengthens the delocalization in the π-electron structure also inducing absorption at higher wavelengths. Figure 1 demonstrates the radical formation as well according to the work of Eslami and co-authors,[34] who studied the oxidation of gallate anions to gallate radicals by using electron paramagnetic resonance (EPR) spectroscopy.

This is a PDF file of an unedited manuscript that has been accepted for publication. Final edited form is published in *Langmuir, 2014, 30:15451−15461*. http://dx.doi.org/10.1021/la5038102

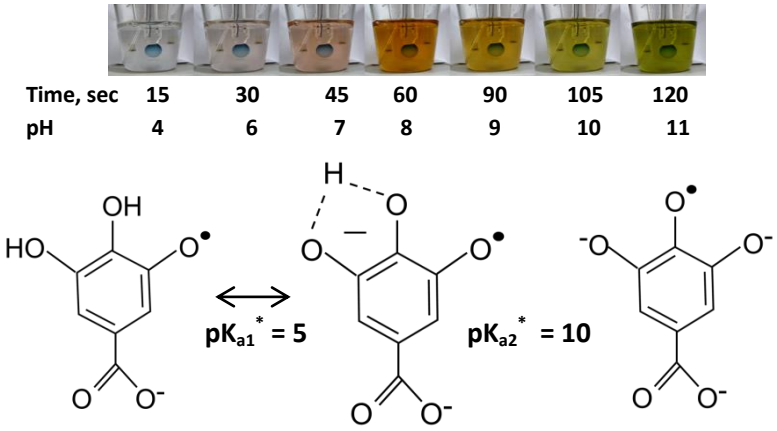

Figure 1. Top: Gradual change in the color of aqueous gallic acid solution after NaOH addition to increase the pH from ~4 to ~11 (the pH-electrode is immersed in the titration vessel). Bottom: The formation of gallate radicals during air-oxidation; the pK_a values are taken from literature [34].

They concluded that the pK_a (acidic dissociation constant) values of phenolic OH groups of the radicals (pK_a^*) were significantly lower compared to known pK_a values of non-oxidized gallate ions: $pK_{a1}^* = 5$ compared to $pK_{a1} = 8.7$ and $pK_{a2}^* = 10$ compared to $pK_{a2} = 11.4$. Thus in the case of radical formation, the latter phenolic OH groups become dissociated at pH~11. The combination of the parallel processes of OH dissociation, radical formation and GA oxidation to hydroquinone, semiquinone and quinone is responsible for the color changes in GA solutions under ambient conditions.

The spectral changes of GA solutions with pH increasing from ~4 to ~11 are presented in Figure 2. Spectra were measured right after pH-adjusting. Different concentrations of GA were needed to resolve the spectra at low and high wavelengths, and so the spectral details below and above 350 nm are presented separately. The typical 265 nm absorption, characteristic of the GA solutions at low pH, shifts to 300 nm with increasing pH (Figure 2A). In the same time, new absorption bands appear at higher wavelengths: 380, 480 and 650 nm (Figure 2B). The first new band at 380 nm is probably due to deprotonation of the carboxyl group of GA ($pK_a = 4.0$)[36] and so it does not induce color change.

This is a PDF file of an unedited manuscript that has been accepted for publication. Final edited form is published in *Langmuir, 2014, 30:15451−15461*. http://dx.doi.org/10.1021/la5038102

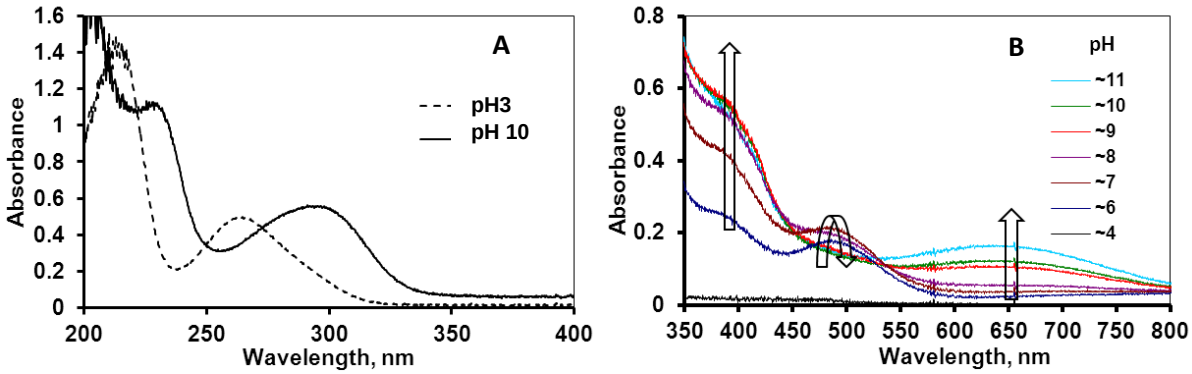

Figure 2. Light absorption spectra of GA in the UV range at pH~3 and ~10 (A) and in the Vis range at pHs ~4 to ~11 (B). The arrows in panel B indicate the direction of pH increase.

The bands at 480 nm and 650 nm are responsible for the orange and green colors of GA solutions, respectively. The gradual transition from orange to green is seen in the spectra also, as the 480 nm band gradually disappears while the intensity of the 650 nm band increases with pH.

The results of the potentiometric acid-base titration experiments are seen in Figure 3. The absolute values of net proton consumption express the molar amount of protons dissociated per 1 g of GA in the course of the titration. The negative sign means OH^- consumption by protons released from GA into the bulk solution. The paths of deprotonation (with pH increasing from 3 to 11, empty dots) and protonation (with pH decreasing from 11 to 3, full dots) differ significantly. This indicates the presence of dissimilar GA species in the opposite directions of pH change. We estimated the pK_a values of the dissociable groups of GA from the derivation of net proton consumption vs. pH curves (dashed and solid red lines for the up and down titrations, respectively). In the direction of increasing pH, the known pK_{a1}=4.0–4.5 of the carboxylic group and pK_{a2}~8.5 of a phenolic OH group of GA in para position[34,36-38] can be identified. In the opposite direction of pH change, however, additional new peaks appear that reflect the protonation of phenolic OH groups with pK_a values of 5.9 and 10.8, closely resembling the values of 5 and 10 found by Eslami and co-authors[34] for GA radicals in EPR studies. FITEQL model calculations were performed to find more accurate pK_a values of GA and GA radicals and to estimate the extent of radical formation. The details of model calculations are given in Supplementary Material (Section 1). In the direction of increasing pH, the model calculation resulted in the values of pK_{a1}(carboxylic

This is a PDF file of an unedited manuscript that has been accepted for publication. Final edited form is published in *Langmuir, 2014, 30:15451−15461*. http://dx.doi.org/10.1021/la5038102

group)=4.3, pK_{a2}(phenolic OH in para position)=8.8 and pK_{a3} (phenolic OHs in meta position)=11.5. Additional pK_a values 6.5 and 9.8 were needed to fit the data in the direction of decreasing pH, which were assigned to the dissociation of phenolic OH groups of GA radicals: pK_{a2}^*=6.5 and pK_{a3}^*=9.8. The calculation shows that ~44 % of the present GA transformed to GA radicals. The pH increase in the presence of oxygen (the O_2 concentration of bubbling N_2 was ~10 ppm) makes the radical formation probable by the end of up titration, which is confirmed by the appearance of the additional pK_a values. The color changes of the GA solution in the course of down titration (pH decreasing from 11 to 3, Figure 3) are similar to those observed during increasing pH (NaOH addition in larger portions, Figure 1) with the important difference that the original colorless solution was not regained by the end of the down titration. Thus, the quinone-hydroquinone transformation was not reversible. It can be supposed that the GA radicals have formed dimers that still persist at low pH and are responsible for the remaining color. Caregnato et al[35] have predicted the recombination of phenoxyl radicals of gallic acid to biphenyls and quinones in DFT (density

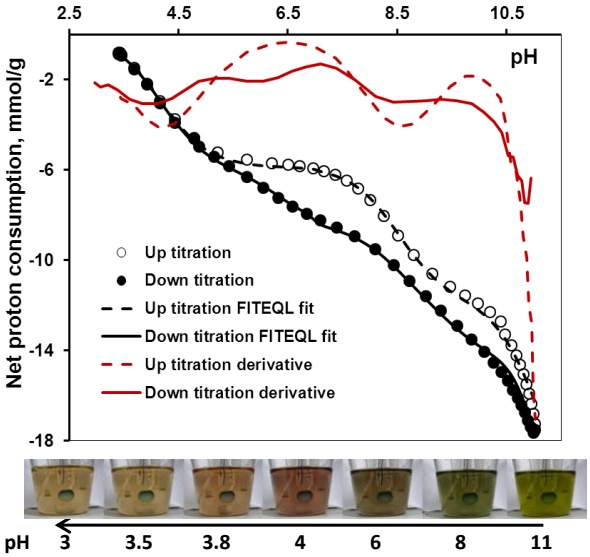

Figure 3. pH-dependent dissociation of gallic acid (dots) with increasing and decreasing pH between 3 and 11 at 0.5 M ionic strength. The pictures demonstrate the changes in the color of GA solution in the course of the down titration (the arrow indicates the direction of pH change from 11 to 3).

This is a PDF file of an unedited manuscript that has been accepted for publication. Final edited form is published in *Langmuir, 2014, 30:15451−15461*. http://dx.doi.org/10.1021/la5038102

functional theory) calculations and observed it experimentally as well. Oniki and Takahama[39] have observed the oxidative C–O coupling of GA at pH between 10.5 and 12 and Nicolic et al[40] have found formation of both C–O and C–C dimers of GA.

We also observed that the color of the GA solutions darkened significantly at all pHs with increasing salt content (Supplementary Material, Section 2) meaning that the concentration of the colored species increases with ionic strength. It is apparent that the background electrolyte can stabilize the electron delocalization in the GA radicals.

We studied the changes in the spectral properties of GA solutions (12 mmol/dm^3 concentration at pHs 2.6, 4.2, 6.1, 8.3, 9.4 and 11) in the course of 5 weeks. The results are shown in Figure 4. The color of the GA solutions became green after 1 day (Figure 4A) and then changed to orange with time (Figure 4B) at all pH values except for 2.1. The UV-Vis spectra recorded after 1 day and 5 weeks standing show the decrease in the intensity of the typical peak at ~265 nm with both increasing pH and time, which is due to the decrease in GA monomer concentration. The separate absorption bands at ~480 and ~650 nm found in the experiment of pH increase within 2 minutes (Figure 2B) cannot be

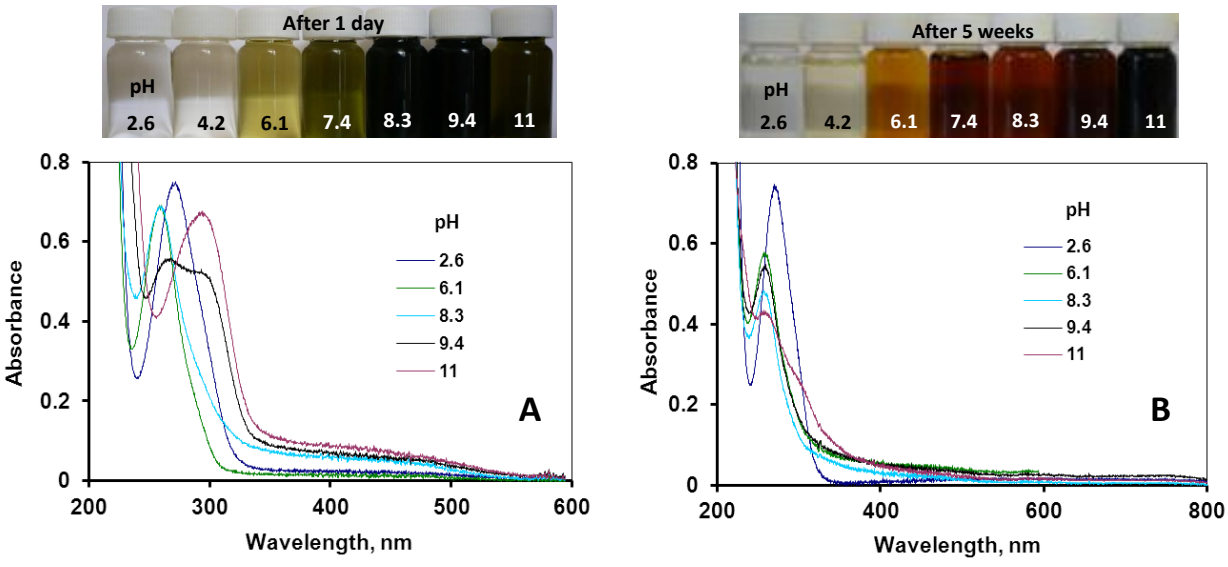

Figure 4. Color of GA solutions (12 mmol/dm^3 concentration in 10 mM NaCl medium) at different pHs and the UV-Vis spectra of the solutions observed after standing for 1 day (A) and 5 weeks (B).

observed in the spectra after 1 day. Instead, a steady increase in absorption is seen at wavelengths between ~330 and ~530 nm. The spectra taken after 5 weeks (Figure 4B) also show increased absorption, but in a wider range, i.e., between ~330 and ~800 nm. This means that the number of GA-species increases with time, giving a featureless UV-Vis spectrum at higher wavelengths as compared to the three distinguishable species (i.e., absorption maxima at 340, 480 and 650 nm seen in Figure 2) found right after the pH adjustment. This extension to the direction of higher wavelengths demonstrates the gradual transition of gallate to humic-like polymer, the latter being characterized with featureless UV-Vis spectra. Deligiannakis and co-workers[41,42] studied the polymerization of GA and GA/PA mixtures (PA – protocatechuic acid) in time under basic conditions. They found no polymerization of GA alone within the duration of their experiments (10 days). Our experiments prove that allowing longer time, formation of some GA oligomers is possible in 5 weeks.

3.2 In-situ surface polymerization of adsorbed GA.

We have proved earlier[8,12,13] that GA adsorbs to MNP via bidentate or bridging complex formation between the surface Fe ions of MNP and the OHs of GA in ortho position. Polymerization of the surface-bound GA was deduced from adsorption isotherms, FTIR-ATR spectra and particle size and surface charge state determination. Additional experiments were necessary to clarify the mechanism of the in situ surface polymerization of GA on MNPs, the results of which are discussed below.

3.2.1 GA adsorption on MNP. The effect of increasing ionic strength and equilibration time on the adsorption isotherms of GA on MNP at pH ~6.5 is shown in Figure 5. Significant increase in the adsorbed amounts of GA is observed, while the main characteristics of the isotherms (i.e., the high-affinity of GA to the MNP surface and the absence of adsorption saturation) do not change. The adsorbed amount at the high-affinity adsorption limit increases from 0.1 mmol/g at 10 mM to 0.2 mmol/g at 100 mM of NaCl (Figure 5A). At 10 mM ionic strength, –0.1 mmol/g of GA carboxylate charge is brought to the surface, while the charge of naked MNPs is ~+0.05 mmol/g.[43] The positive surface charge of MNPs is doubly overcompensated by the adsorbed GA charges. The latter picture is

This is a PDF file of an unedited manuscript that has been accepted for publication. Final edited form is published in *Langmuir, 2014, 30:15451−15461*. http://dx.doi.org/10.1021/la5038102

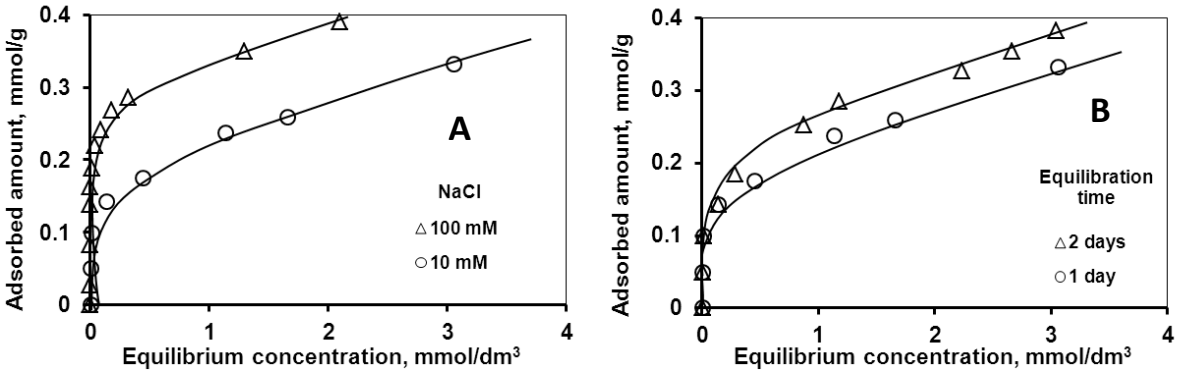

Figure 5. Adsorption isotherms of GA on MNP measured at pH ~6.5 after 1 day of equilibration at –10 (o) and 100 (Δ) mM ionic strengths (A) and after 1 day (o) and 2 days (Δ) of equilibration at 10 mM ionic strength (B). The reproducibility was ±0.05 mmol/g. The error bars are omitted for clarity. The lines are drawn to guide the eyes.

characteristic of specific ion adsorption, i.e., chemisorption, fully supported by the bidentate or bridging Fe-GA surface complex formation similar to catecholate-bonds.[44] In accordance with this, electrophoretic mobility measurements[12] revealed that the zeta potential of the GA@MNPs at this state is ~ –25 mV.

Above the high-affinity adsorption limit, the isotherm shows the characteristic shape of adsorption with equilibrium distribution of GA between the adsorbed and dissolved states. In this state, the role of the ionic strength is to screen the charge of the adsorbed layer. Significantly higher overcharge (about –0.15 mmol/g) could be achieved at the high affinity limit of GA adsorption in 100 mM NaCl (~0.2 mmol/g) due to the enhanced screening effect of the electrolyte. The fact that the adsorbed amounts do not reach saturation value (i.e., the plateau is absent in the isotherms) hints that there are other equilibria in the system as well in addition to adsorption. The actual adsorption should have ended at the stage of monolayer coverage because of the limited amount of ≡Fe–OH sites available for surface complexation with GA via bidentate chelate formation.[12,13,22] It is likely that surface polymerization of GA takes place. GA in the adsorbed state exposes a free OH group and a carboxylic group prone to polycondensation reaction with GA in the medium. The probability of the polymerization of adsorbed GA is supported by

the gradual increase of the adsorbed amount both with concentration and time, as it is shown in Figure 5B. After 2 days of equilibration, the adsorbed amounts increased undoubtedly relative to that after the first day. The high-affinity limit of the adsorption, however, did not increase with time revealing that the time-dependent change does not affect the amount of GA bound directly to the surface ≡Fe–OH sites. Instead, GA monomers from the bulk are likely to bind to the previously adsorbed molecules. Additional dynamic light scattering experiments show that the hydrodynamic diameter of the MNPs increases gradually with time from ~100 nm (characteristic of uncoated MNPs) to ~170 nm (characteristic of polyelectrolyte coated MNPs). Our results suggest that the thickness of the GA coating can be easily controlled by the added amount of GA and time of equilibration. For example, at 0.6 mmol/g GA addition, the evolution of the thickness to the maximal value obtained in our experiments (~170 nm hydrodynamic diameter of the polyelectrolyte-coated MNPs) can be achieved during 4 weeks, while the same thickness is reached within 2 weeks when the added amount of GA is 10 mmol/g. The data are presented in Section 3 of Supplementary Material. We should note that the size of magnetic cores did not change in the meantime (see TEM pictures and particle size distributions in Section 4 of Supplementary Material).

GA desorption experiments were performed to test the resistance of the coating layer to dilution representing the changes in the solid/liquid ratio due to administration of coated MNPs in possible biomedical applications. After the adsorption equilibrium was achieved, we decreased the GA concentration to half of the initial one and measured the new solution concentrations established in the course of 24 h. Desorption of GA in response to the dilution is the direct measure of the interfacial stability of the adsorbed layer. The comparison of the adsorption and desorption isotherms (see in Section 5 of Supplementary Material) reveals that the adsorbed amounts of GA practically did not change during dilution. The GA shell essentially remained intact after dilution resembling the well-known stability of humic coating on mineral particles occurring in environmental compartments, such as water, sediment or soil.

This is a PDF file of an unedited manuscript that has been accepted for publication. Final edited form is published in *Langmuir, 2014, 30:15451−15461*. http://dx.doi.org/10.1021/la5038102

3.2.2 Surface induced polymerization of GA. UV-Vis spectra of the supernatant GA solutions of selected adsorption systems ($c_{0,GA}$=0.0011, 0.0024, 0.092 and 0.32 mmol/dm^3) were taken after one day and one week of adsorption time. After 1 day of equilibration, the supernatants obtained a dark purple color (Figure 6A). A broad absorption band appeared in the spectra centered at ~600 nm, which is characteristic of Fe^{2+} [17, 45] or Fe^{3+} [46, 47] chelates of gallic acid. The dark purple color resembles that of the famous gall ink.[48] Here, it indicates the presence of trace Fe^{2+}or Fe^{3+} ions in the medium of the magnetite dispersion dissolved from the crystalline phase. The absorption band of the GA aromatic ring at ~260 nm remains well resolved in the spectrum. The color of the iron–GA complex disappeared with time (Figure 6B), presumably owing to the continual adsorption of GA on the surface, as it is also demonstrated by the increased amounts of adsorption with time (Figure 5B). In addition, the color of the supernatant solutions reveals that not the entire amount of GA is adsorbed on the surface. The spectra of the supernatant solutions is featureless and the absorbance decreases continuously with increasing wavelength at each concentration similarly to the spectra of humic and humic-like substances.[42] The color ratio defined as the measured absorbance value at 400 nm (E4) divided by that at 600 nm (E6) was calculated at the highest GA concentration as E4/E6=4.3.

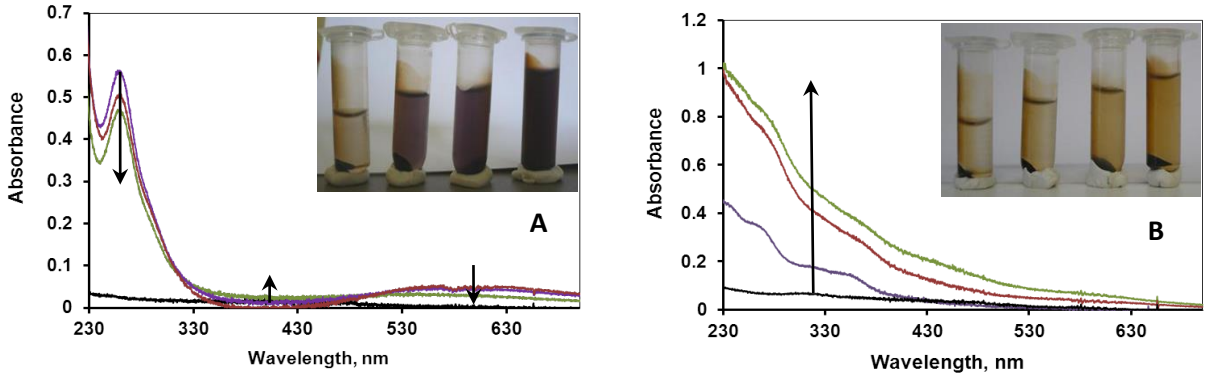

Figure 6. Pictures of selected GA/MNP adsorption systems at pH~6.5 and 10 mM NaCl after 1 day (A) and 1 week (B) of equilibration, together with the UV-VIS spectra of the supernatants. The initial concentrations of GA are denoted by black, purple, brown and green lines in increasing order.

In general, the value of the E4/E6 ratio is 3–5 for humic acids and ≥8 for fulvic acids[49] the most abundant organic polyacids in nature, the color of which changes from yellowish-brown to black depending on the degree of polymerization. The increase in the adsorbed amount with time (Figure5B) and the darkening of the supernatant solution (Figure 6B) suggest that GA polymerization proceeds both at the surface of MNP and in solution. GA did not polymerize easily in the absence of MNPs (Section 3.1), and so this result shows that the presence of iron ions in the solution phase can promote GA polymerization. Both the solution polymerization in the presence of iron ions and the surface induced polymerization are probably due to the destabilization of gallate radicals formed at pH~6.5 in the presence of oxygen. In addition, we measured the pH-dependence of the hydrodynamic diameter of GA@MNPs at 1 day and 4 weeks after preparation. Graphical representation of the results is given in Section 6 of Supplementary Material. In general, the GA coating becomes protonated at low pH ($<pK_{a1}$=4–5) giving rise to particle aggregation with aggregate sizes of several thousand nm, but with increasing pH, GA becomes dissociated and stabilizes the primary particles electrostatically. After 1 day of GA adsorption, the hydrodynamic diameter of the GA-coated particles at high pH is close to that of naked MNPs (~100 nm) published by us earlier.[12] However, it approaches the value of ~170 nm four weeks after the preparation, characteristic to that of polyelectrolyte (polyacrylic acid[50] and poly(acrylic-co-maleic acid[43]) coated MNPs. This reveals that the surface polymerization of GA proceeds with time. We have earlier deduced the high probability of the formation of polygallate coating layer on the MNPs (PGA@MNP) indirectly from particle size and particle size distribution measurements of GA-coated MNPs.[12,13]

The effect of the formation of a PGA shell on the salt tolerance of the core-shell MNPs was measured in coagulation kinetics experiments. The aggregation of nanoparticles was measured in time as the increase in the hydrodynamic diameter of scattering units at gradually increasing electrolyte concentrations. The stability plots in Figure 7 show that adding GA to the MNPs at concentration of 10 mmol/g increases the value of critical coagulation concentration (CCC) from 1 mM (naked MNP) to ~100 mM as measured 1 day after the start of GA adsorption. As GA surface polymerization continues

This is a PDF file of an unedited manuscript that has been accepted for publication. Final edited form is published in *Langmuir, 2014, 30:15451−15461*. http://dx.doi.org/10.1021/la5038102

for 1 day (Figure 6), the increase in the salt tolerance is caused by electrostatic stabilization due to adsorbed GA monomers carrying dissociated carboxylic groups. The size of the electrostatically

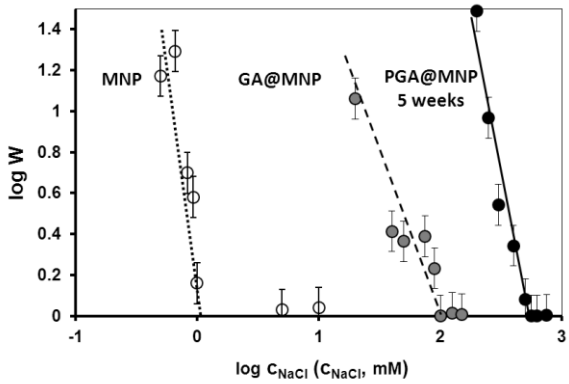

Figure 7. Determination of the salt tolerance of naked MNP and GA-coated MNPs (10 mM GA/g MNP) 1 day (GA@MNP) and 5 weeks (PGA@MNP) after preparation. The pH is ~6.5. The CCC values are seen as the intersection points of the log W vs. log c_{NaCl} lines of the slow coagulation regime with the x-axis.

well stabilized MNPs with adsorbed and dissociated gallate anions is practically the same as that of the naked MNPs (Section 6 of Supplementary Material). Because the CCC is lower than the physiological salt concentration (154 mM), the adsorbed monolayer of GA – sufficient for electrostatic stabilization – cannot protect the particles from aggregation at higher salt concentrations. In contrast, the PGA@MNPs formed during 5 weeks resist salt induced coagulation up to ~500 mM concentration of NaCl. This remarkable salt tolerance is due to electrosteric stabilization, the combined effect of high surface charge density and thick layer of PGA coating.

3.2.3 XPS study of GA surface polymerization. The high resolution XPS spectra of O, C and Fe in a PGA@MNP sample standing for 4 weeks after preparation are shown in Figure 8. The peaks are deconvoluted into the components. The fitting parameters of the deconvolution (the peak positions (binding energy) and the full width at half maximum (FWHM)) together with the atomic concentrations calculated from peak areas are given in Table 1. We have detected an unusually high concentration of

This is a PDF file of an unedited manuscript that has been accepted for publication. Final edited form is published in *Langmuir, 2014, 30:15451−15461*. http://dx.doi.org/10.1021/la5038102

inorganic carbonate in the original sample supposedly because of prolonged ageing at ambient conditions. To remove the carbonate, the sample was acidified to pH~4 and the pH was subsequently set back to ~6.5.

As it is seen in the O 1s spectra, the original PGA@MNP sample loses its adsorbed water after acidifying, which is explained by the dehydration due to suppressed dissociation of carboxylate groups at low pH. The Fe^{3+}/Fe^{2+} atomic ratio at the surface of PGA-coated MNPs as calculated from the Fe^{3+} and Fe^{2+} 2p peak areas decreased to 1.77 from its original value of 2 in bulk magnetite ($Fe(III)_2Fe(II)O_4$), which shows the reduction of iron at the MNP surface in the presence of gallic acid. The C 1s peaks of the PGA@MNPs were assigned to aromatic carbons (C–C, 284.72 eV), phenolic OH groups (C–O, 285.6 eV, alcohols/ ethers), carboxylic groups (O=C–O, 288.87 eV, carboxylic acids/esters) and carbonates ($O=CO_2$, 290.58 eV), according to Nevskaia et al,[51] Desimoni et al[52] and Martin et al.[53] The carbonate contamination of the original PGA@MNP (290.58 eV in Table 1) due to the prolonged surface polymerization process under ambient conditions could be successfully removed by acidifying the dispersions to pH~4 using HCl (Figure 8, bottom row). The O=C–O/C–O ratio calculated from the C 1s peak areas is 0.675, about twice the value of the GA molecule 0.33.

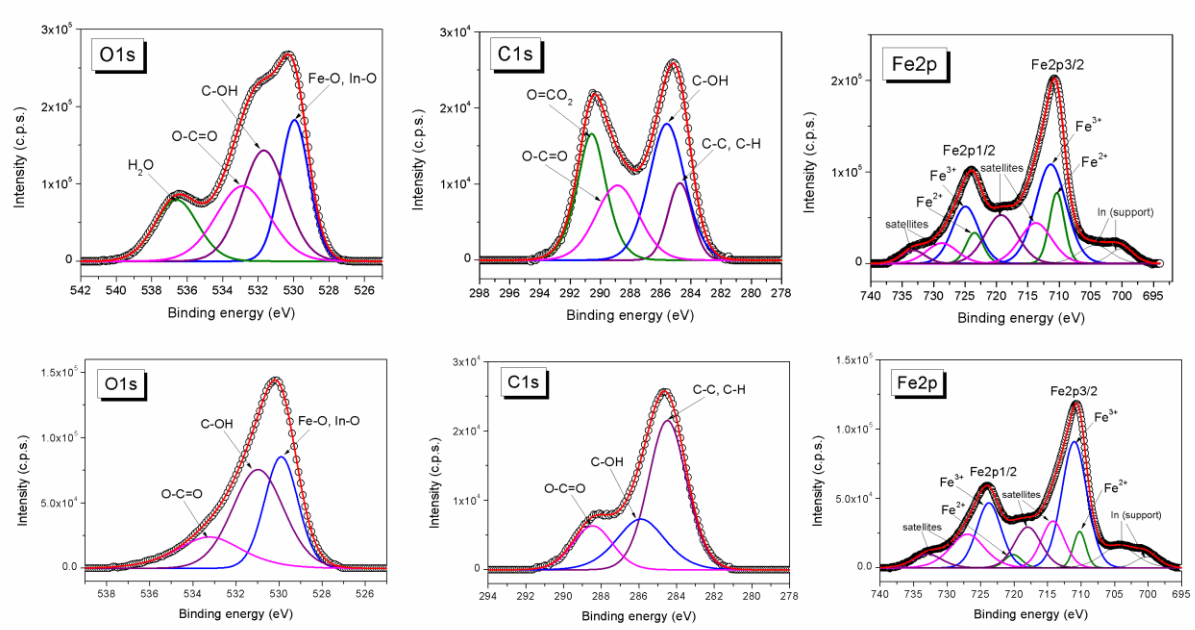

Figure 8. O 1s, C 1s and Fe 2p spectra of the original (top row) and acidified PGA@MNPs (bottom row) aged for 4 weeks at pH~6.5 and 10 mM NaCl.

This is a PDF file of an unedited manuscript that has been accepted for publication. Final edited form is published in *Langmuir, 2014, 30:15451−15461*. http://dx.doi.org/10.1021/la5038102

This result shows that some phenolic groups of GA become oxidized to carboxylates in the adsorbed state. This oxidation, in addition, proceeds on account of iron reduction, as it is evidenced by the decreased Fe^{3+} / Fe^{2+} ratio of the PGA@MNPs. The reducing property of GA has been studied in EPR experiments.[34] We have also demonstrated the excellent passivizing efficiency of PGA coating on MNPs in iron dissolution studies measured by ICP (inductively coupled plasma) analysis.[8] The present XPS results support the earlier findings and elucidate the exact mechanism of chemical stabilization of iron oxide nanoparticles by PGA coating. Chemical stability of core-shell magnetite nanoparticles is necessary to avoid the detrimental effects of dissolved Fe ions in tissues and cells[8-10] and so it is of primary importance for their biomedical applicability in future.

Table 1. Assignment of peaks in the XPS spectra of the original and acidified PGA@MNPs together with binding energies (Position, eV), peak breadth (FWHM, eV) and atomic concentration percentages (Atomic Conc. %).

Peak name	PGA@MNP			PGA@MNP acidified		
	Position (eV)	FWHM (eV)	Atomic conc. (%)	Position (eV)	FWHM (eV)	Atomic conc. (%)
Fe^{2+} 2p3/2	710.38	2.807	2.725	710.25	2.185	1.511
Fe^{3+} 2p3/2	711.35	5.752	7.839	711.05	4.423	10.628
Fe^{2+} 2p1/2	723.47	3.224	2.638	720.18	3.011	1.461
Fe^{3+} 2p1/2	724.94	5	7.591	723.79	4.3	10.289
Fe^{2+} satellite 2p3/2	713.73	6	3.349	714.24	4.062	3.616
Fe^{3+} satellite 2p3/2	719.25	6	4.008	717.99	4.681	3.638
Fe^{2+} satellite 2p1/2	728.69	5.794	3.156	727.02	6	7.652
Fe^{3+} satellite 2p1/2	733.24	4.485	1.587	732.9	5.053	2.596
C 1s ; C-C, CH	284.72	1.896	2.33	284.49	2.375	13.143
C 1s; C-OH	285.6	2.786	6.177	285.9	3.03	5.827
C 1s; O=C-O	288.87	3.356	4.028	288.46	2.461	3.994
C 1s; $O=CO_2$	290.58	2.265	4.789	-	-	-

This is a PDF file of an unedited manuscript that has been accepted for publication. Final edited form is published in *Langmuir, 2014, 30:15451−15461*. http://dx.doi.org/10.1021/la5038102

O 1s; Fe-O, In-O	529.96	1.92	12.951	529.9	1.832	12.142
O 1s; C-OH	531.69	2.918	15.569	530.98	2.802	16.555
O 1s; O=C-O	532.88	3.557	12.867	533.24	3.566	6.947
O 1s; H_2O	536.62	2.857	8.431	-	-	-

3.2.4 The mechanism of GA surface polymerization on MNPs. Our FTIR-ATR results[13] have shown that GA polymerization proceeds on the MNP surface via ester and/or ether linkages represented in Section 7 of the Supplementary Material, proven by the appearance of characteristic absorption in the frequency range 1700-1750 cm^{-1}. It is shown by ESR (electron spin resonance) spectra[39] that dimerization is possible at high pH via C–O–C bridging after oxidation of GA to semiquinone radicals. The latter ether formation reaction occurs between phenolic groups belonging to different GA molecules. The FTIR-ATR spectrum of PGA@MNPs measured four weeks after preparation is presented in Figure 9 together with the spectra of pure GA and GA@MNPs 1 day after preparation. Three important changes in the spectrum can be observed with time. First, a new strong band appears at 1650 cm^{-1}, characteristic of the presence of quinones and/or conjugated ketones (red label in Figure 9).

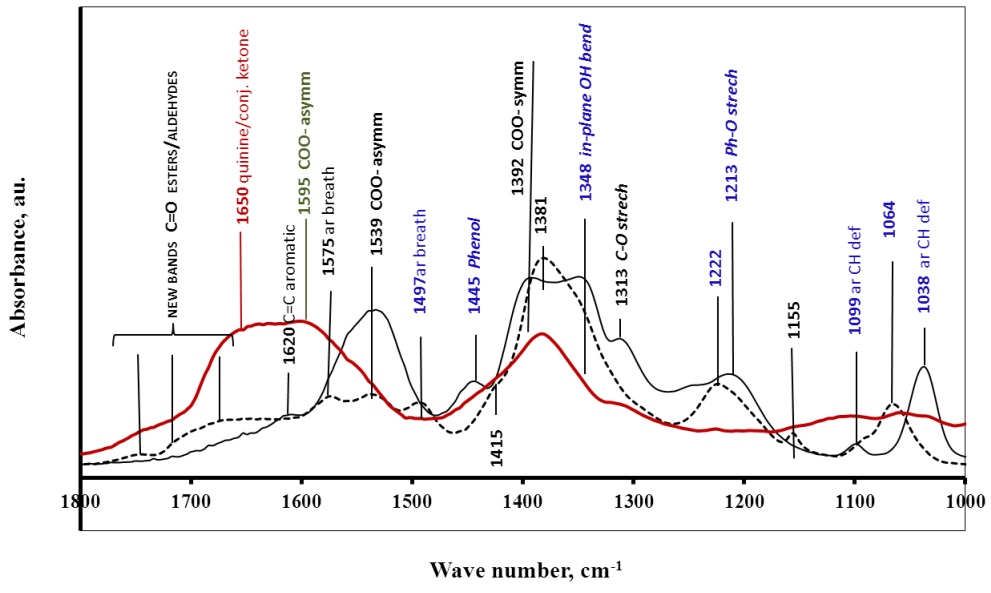

Figure 9. FTIR-ATR spectra of GA (black solid line), GA@MNP measured 1 day after its preparation (black dashed line) and PGA@MNP measured 4 weeks after preparation (red solid line). The changes

in the spectrum owing to GA → PGA surface polymerization are labeled in red, green and blue. The black labeled bands are due to the adsorption of GA on MNP.[13]

The latter are clear signs of GA oxidation. The second change is that the asymmetric stretching band of $–COO^-$ becomes shifted from 1539 to 1595 cm^{-1} (green label in Figure 9). This unusually large shift can be the consequence of significant changes in the molecular environment of the carboxylates. The electrokinetic potential and XPS results clearly demonstrate the presence of a large amount of carboxylic groups in the PGA@MNP samples. The doubling in the carboxylic content (O=C–O vs C–O) seen in the XPS spectra implies that although the original carboxylic groups enter ester binding in surface polymerization, new carboxyls form probably on all GA monomers as a result of oxidation. Thus, the large shift of the asymmetric $–COO^-$ stretching band from 1539 to 1595 cm^{-1} is more likely than its complete disappearance from the spectrum. However, new carboxylic groups can only form in a ring opening mechanism resulting in a changed structure of the original GA molecules from aromatic to aliphatic. In phenol degradation experiments,[54,55] several examples can be found for the enzymatic and heterogeneous catalytic oxidation of phenols to various aliphatic acids as reaction intermediates. The third and most important change in the FTIR spectrum is the complete disappearance of all bands associated with the aromatic character of the GA molecules (blue labels in Figure 9), which in turn proves that the ring opening mechanism occurs indeed in the process of surface induced polymerization of GA on MNPs. The disappearance of C=C aromatic bands (1620 cm^{-1}) and one of the two aromatic breathing modes (1575 cm^{-1}) cannot be proven from the experiments because these are buried under the envelopes of the 1650 and 1595 cm^{-1} bands (quinone/conjugated ketones and $–COO^-$ asymmetric stretching, respectively). Nevertheless, these are also likely vanished together with the other aromatic bands of GA and GA@MNP at 1038, 1064, 1099, 1213, 1222, 1348, 1445 and 1497 cm^{-1}.

We have shown[12] that the negative electrokinetic potential of MNPs increases significantly with

This is a PDF file of an unedited manuscript that has been accepted for publication. Final edited form is published in *Langmuir, 2014, 30:15451−15461*. http://dx.doi.org/10.1021/la5038102

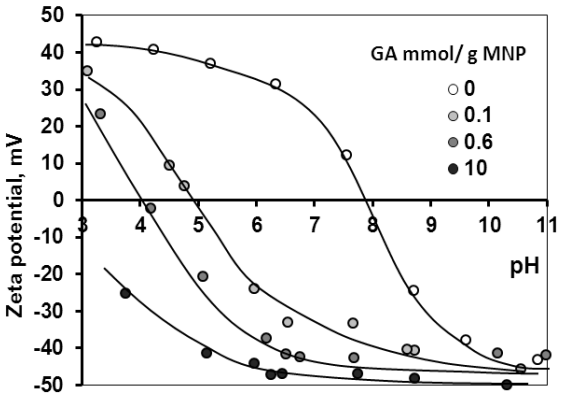

Figure 10. pH-dependence of the electrokinetic potential of GA@MNPs aged for 1 day in function of the added amount of GA. The pH of the isoelectric point decreases from ~8 (uncoated MNP) to ~5, ~4 and <~3 with increasing GA loading. The lines are drawn to guide the eyes. The accuracy of zeta potential values is ±5 mV (the error bars are omitted for clarity).

GA adsorption at pH~6.5. The changes in the electrokinetic potential of MNPs measured 1 day after GA adsorption at varying pH values are shown in Figure 10. Surface polymerization of GA begins right after its adsorption and so the data are characteristic of the polymerization process as well. In the presence of GA, the decrease in the pH of the isoelectric point is observed also above the high-affinity adsorption limit, 0.1 mmol/g. This would imply the formation of ether but not ester bridges, since the number of surface carboxylate groups increases clearly in the process of surface polymerization although it should remain unchanged in case of ester formation. On the other hand, ester formation, in general, should be the preferred reaction. This apparent contradiction becomes interpretable in the light of the XPS results.

The present XPS results clearly show that the increase in the carboxylate groups during GA adsorption is the result of a redox process between surface iron ions and gallic acid: the phenolic OH groups become oxidized to carboxylates via ring opening on the expense of iron reduction (Fe^{3+} to Fe^{2+}). Thus, GA polymerization can proceed via the thermodynamically more probable esterification reaction, while the amount of dissociated carboxyl groups necessary for electrostatic stabilization of the MNPs increases due to GA oxidation.

4. Conclusions

We proved the formation of polygallate-coated MNPs in the process of surface induced polymerization of the GA adsorbed on iron oxide. This process takes place spontaneously under mild conditions (i.e., room temperature, aqueous medium, pH~6.5) in the presence of Fe^{3+}/Fe^{2+} redox couple and the magnetite surface as catalyst. The same type of reactions can be found in the environment between clay and/or metal oxide particles and various small molecular weight organic molecules, which inspired a new way to synthesize core-shell MNPs . Similar to the humic or fulvic acid coated minerals, the prepared PGA@MNPs possess great chemical stability, making them highly preferable for biomedical applications relative to the most of other type core-shell MNPs.

Rational combination of the results of adsorption, dynamic light scattering, potentiometric acid-base titration, electrokinetic potential measurements, FTIR-ATR, UV-Vis and XPS experiments allowed us to prove the mechanism of the surface induced polymerization of GA. We found that polymerization proceeds mainly via ester binding between surface bound and free GA radicals with the participation of carboxyl and phenolic OH groups. The consumption of dissociable carboxyl groups would prevent the development of high negative surface charge density of the PGA coating, however, as XPS reveals additional phenolic OH groups become oxidized on the account of Fe^{3+} reduction to create new carboxylic groups through ring opening mechanism.

Gallic acid is a potent antioxidant either in the monomeric or polymerized state;[37] thus, it is worth testing the biological activity of PGA@MNPs in *in vitro/in vivo* tests, which together with their MRI contrast enhancement and hyperthermia efficiency is the topic of our subsequent publication.

Acknowledgement

This work has been supported by the Hungarian Scientific Research Found OTKA (NK84014).

References

(1) Chatterjee, K.; Sarkar, S.; Rao, K. J.; Paria, S. Core/shell nanoparticles in biomedical applications. *Adv. Colloid Interface Sci.* **2014**, *209*, 8–39.

(2) Ladj, R.; Bitar, A.; Eissa, M. M.; Fessi, H.; Mugnier, Y.; Le Dantec, R.; Elaissari, A. Polymer encapsulation of inorganic nanoparticles for biomedical applications. *Int. J. Pharm*. **2013**, *458*, 230–241.

(3) Figuerola, A.; Di Corato, R.; Manna, L.; Pellegrino, T. From iron oxide nanoparticles towards advanced iron-based inorganic materials designed for biomedical applications. *Pharmacol. Res.* **2010**, *62*, 126–143.

(4) Mahmoudi, M.; Sant, S.; Wang, B.; Laurent, S.; Sen, T. Superparamagnetic iron oxide nanoparticles (SPIONs): Development, surface modification and applications in chemotherapy. *Adv. Drug Delivery Rev*. **2011**, *63*, 24–46.

(5) Kumar, C. S. S. R.; Mohammad, F. Magnetic nanomaterials for hyperthermia-based therapy and controlled drug delivery. *Adv. Drug Delivery Rev*. **2011**, *63*, 789–808.

(6) Gupta, A. K.; Gupta, M. Synthesis and surface engineering of iron oxide nanoparticles for biomedical applications. *Biomaterials* **2005**, *26*, 3995–4021.

(7) Dufort, S.; Sancey, L.; Coll, J. L. Physicochemical parameters that govern nanoparticles fate also dictate rules for their molecular evolution. *Adv. Drug Delivery Rev*. **2012**, *64*, 179–189.

(8) Szekeres, M.; Tóth, I. Y.; Illés, E.; Hajdú, A.; Zupkó, I.; Farkas, K.; Oszlánczi, G.; Tiszlavicz, L.; Tombácz, E. Chemical and colloidal stability of carboxylated core-shell magnetite nanoparticles designed for biomedical applications. *Int. J. Mol. Sci*. **2013**, *14*, 14550-14574.

(9) Soenen, S. J.; Himmelreich, U.; Nuytten, N.; Pisanic, T. R.; Ferrari, A.; de Cuyper, M. Intracellular nanoparticle coating stability determines nanoparticle diagnostics efficacy and cell functionality. *Small* **2010**, *6*, 2136–2145.

(10) Soenen, S. J..; Himmelreich, U.; Nuytten, E.; de Cuyper, M. Cytotoxic effects of iron oxide nanoparticles and implications for safety in cell labelling. *Biomaterials* **2011**, *32*, 195–205.

(11) Soenen, S. J.; Nuytten, N.; Himmelreich, U.; de Cuyper, M. Intracellular iron oxide nanoparticle coating stability determines nanoparticle usability and cell functionality. *Drug Discovery Today* **2010**, *15*, 1082.

(12) Tombácz, E.; Tóth, I. Y.; Nesztor, D.; Illés, E.; Hajdú, A.; Szekeres, M.; Vékás, L. Adsorption of organic acids on magnetite nanoparticles. pH-dependent colloidal stability and salt tolerance, *Colloids Surf., A* **2013**, *435*, 91–96.

(13) Tombácz, E.; Szekeres, M.; Hajdú, A.; Tóth, I. Y.; Bauer, R. A.; Nesztor, D.; Illés, E.; Zupkó, I.; Vékás, L. Colloidal stability of carboxylated iron oxide nanomagnets for biomedical use. *Period. Polytech., Chem. Eng.* **2014**, *58*, 3–10.

(14) Yilmaz, Y.; Toledo, R. T. Major flavonoids in grape seeds and skins: Antioxidant capacity of catechin, epicatechin, and gallic acid. *J. Agric. Food Chem*. **2004**, *52*, 255–260.

(15) Chvátalová, K.; Slaninová, I.; Brezinová, L.; Slanina, J. Influence of dietary phenolic acids on redox status of iron: Ferrous iron autoxidation and ferric iron reduction. *Food Chem*. **2008**, *106*, 650–660.

(16) Domingo, J. L.; Ortega, A.; Llobet, J. M.; Corbella, J. Effectiveness of chelation therapy with time after acute uranium intoxication. *Fundam. Appl. Toxicol*. **1990**, *14*, 88–95.

(17) Lu, L.-l.; Li, Y.-h.; Lu, X.-y. Kinetic study of the complexation of gallic acid with Fe(II). *Spectrochim. Acta, Part A* **2009**, *74*, 829–834.

(18) Bose, P.; Bose, M. A.; Kumar, S. Critical evaluation of treatment strategies involving adsorption and chelation for wastewater containing copper, zinc and cyanide. *Adv. Environ. Res.* **2002**, *7*, 179–195.

(19) Gamage, A.; Shahidi, F. Use of chitosan for the removal of metal ion contaminants and proteins from water. *Food Chem.* **2007**, *104*, 989–996.

(20) Kryvoruchko, A.; Kornilovich, B.; Yurlova, L. Purification of water containing heavy metals by chelating-enhanced ultrafiltration. *Desalination* **2002**, *144*, 243–248.

(21) Kumar, P.; Dara, S. S. Utilisation of agricultural wastes for decontaminating industrial/domestic wastewaters from toxic metals. *Agric. Wastes* **1982**, *4*, 213–223.

(22) Araujo, P. Z.; Morando, P. J.; Blesa, M. A. Interaction of catechol and gallic acid with titanium dioxide in aqueous suspensions. 1. Equilibrium Studies. *Langmuir* **2005**, *21*, 3470–3474.

(23) Colarieti, M. L.; Toscano, G.; Ardi, M. R.; Greco Jr., G. Abiotic oxidation of catechol by soil metal oxides. *J. Hazard Mater.* **2006**, *134*, 161–168.

(24) Wang, T. S. C.; Li, S. W. Clay minerals as heterogeneous catalysts in preparation of model humic substances. *J. Plant Nutr. Soil Sci.* **1977**, *140*, 669–676.

(25) Wang, T. S. C.; Kao, M. M.; Huang, P. M. The effect of pH on the catalytic synthesis of humic substances by illite. *Soil Sci*. **1980**, *129*, 333–338.

(26) Wang, T. S. C.; Wang, M. C.; Ferng, Y. L.; Huang, P. M. Catalytic synthesis of humic substances by natural clays, slits and soils. *Soil Sci*. **1983**, *135*, 350–360.

(27) Chen, Y. M.; Tsao, T. M.; Liu, C. C.; Huang, P. M.; Wang, M. K. Polymerization of catechin catalyzed by Mn-, Fe- and Al-oxides. *Colloids Surf., B* **2010**, *81*, 217–223.

(28) Tombácz, E.; Gilde, M.; Ábrahám I.; Szántó, F. Effect of sodium chloride on interactions of fulvic acid and fulvate with montmorillonite. *Appl. Clay Sci.* **1990**, *5*, 101–112.

(29) Cornell, R. M.; Schwertmann, U. The iron oxides: Structure, properties, reactions, occurrencies and uses. Wiley-VCH: Weimheim, 1996, pp 345–363.

(30) Sun, Z.; Su, F.; Forsling, W.; Samskog, P. Surface Characteristics of Magnetite in Aqueous Suspension. *J. Colloid Interface Sci*. **1998**, *197*, 151–159.

(31) Illés, E.; Tombácz, E. The role of variable surface charge and surface complexation in the adsorption of humic acid on magnetite. *Colloids Surf., A* **2003**, *230*, 99–109.

(32) Szekeres, M.; Tombácz, E. Surface charge characterization of metal oxides by potentiometric acid–base titration, revisited theory and experiment. *Colloids Surf., A* **2012**, *414*, 302–313.

(33) Friedman, M.; Jürgens, H. S. Effect of pH on the Stability of Plant Phenolic Compounds. *J. Agric. Food Chem.* **2000**, *48*, 2101–2110.

(34) Eslami, A. C.; Pasanphan, W.; Wagner, B. A.; Buettner, G. R. Free radicals produced by the oxidation of gallic acid: An electron paramagnetic resonance study. *Chem. Cent. J.* **2010**, *4*, 15. http://journal.chemistrycentral.com/content/4/1/15 (accessed on 27-11-2014)

(35) Caregnato, P.; Gara, P. M.; Bosio, G. N.; Gonzalez, M. C.; Russo, N.; Michelini, M. C.; Mártire, D. O. Theoretical and experimental investigation on the oxidation of gallic acid by sulfate radical anions. *J. Phys. Chem. A* **2008**, *112*, 1188–1194.

(36) Jovanovic, S. V.; Hara, Y.; Steenken, S.; Simic, M. G. Antioxidant potential of gallocatechins. A pulse radiolysis and laser photolysis study. *J. Am. Chem. Soc.* **1995**, *117*, 9881–9888.

(37) Sławińska, D.; Polewski, K.; Rolewski, P.; Sławiński, J. Synthesis and properties of model humic substances derived from gallic acid. *Int. Agrophys*. **2007**, *21*, 199–208.

(38) Abichandani, C. T.; Jatkar, S. K. K. Dissociation constants of ortho-, meta-, and para-hydroxy benzoic acids, gallic acid, catechol, resorcinol, hydroquinone, pyrogallol, and phloroglucinol. *J. Indian Inst. Sci.* **1938**, *21(A)*, 417–441.

(39) Oniki, T.; Takahama, U. Free radicals produced by the oxidation of gallic acid and catechin derivatives. *J. Wood Sci.* **2004**, *50*, 545–547.

(40) Nikolić, G.; Veselinović, A.; Mitić, Ž.; Živanović, S. HPLC-DAD study of gallic acid autoxidation in alkaline aqueous solutions and the influence of Mg(II) Ion. Acta Fact. Med. Naiss. **2011**, *28*, 219–224. http://www.medfak.ni.ac.rs/acta%20facultatis/2011/4-2011/4.pdf (accessed on 27-11-2014)

(41) Giannakopoulos, E.; Drosos, M.; Deligiannakis, Y. A humic-acid-like polycondensate produced with no use of catalyst. *J. Colloid Interface Sci.* **2009**, *336*, 59–66.

(42) Drosos, M.; Jerzykiewicz, M.; Louloudi, M.; Deligiannakis, Y. Progress towards synthetic modelling of humic acid: Peering into the physicochemical polymerization mechanism. *Colloids Surf., A* **2011**, *389*, 254–265.

(43) Tóth, I. Y.; Illés, E.; Bauer, R. A.; Nesztor, D.; Szekeres, M.; Zupkó I.; Tombácz, E. Designed polyelectrolyte shell on magnetite nanocore for dilution-resistant biocompatible magnetic fluids, *Langmuir* **2012**, *28*, 16638−16646.

(44) Ata, M. S.; Liu Y.; Zhitomirsky, I. A review of new methods of surface chemical modification, dispersion and electrophoretic deposition of metal oxide particles. *RSC Adv*. **2014**, *4*, 22716−22732.

(45) Van Leeuwen, Y. M.; Velikov, K. P.; Kegel, W. K. Colloidal stability and chemical reactivity of complex colloids containing $Fe3^{+}$. *Food Chem*. **2014**, *155*, 161–166.

(46) Hynes, M. J.; Coinceanainn, M. O. The kinetics and mechanisms of the reaction of iron(III) with gallic acid, gallic acid methyl ester and catechin. *J. Inorg. Biochem*. **2001**, *85*, 131–142.

(47) Andjelković, M.; Van Camp, J.; De Meulenaer, B.; Depaemelaere, G.; Socaciu, C.; Verloo, M.; Verhe, R. Iron-chelation properties of phenolic acids bearing catechol and galloyl groups. *Food Chem.* **2006**, *98*, 23–31.

(48) Ciglanská, M.; Jancovicová, V.; Havlínová, B.; Machatová, Z.; Brezová, V. The influence of pollutants on accelerated ageing of parchment with iron gall inks. *J. Cult. Herit.* **2014**, *15*, 373–381.

(49) Tan, K. H. Humic matter in soil and the environment. Principles and controversies. Marcel Dekker: New York, 2003, p 177.

(50) Hajdú, A.; Szekeres, M.; Tóth, I. Y.; Bauer, R. A.; Mihály, J.; Zupkó, I.; Tombácz, E. Enhanced stability of polyacrylate-coated magnetite nanoparticles in biorelevant media. *Colloids Surf., B* **2012**, *94*, 242–249.

(51) Nevskaia, D. M.; Martín-Aranda, R. M. Nitric acid-oxidized carbon for the preparation of esters under ultrasonic activation. *Catal. Lett.* **2003**, *87*, 143–147.

(52) Desimoni, E.; Casella, G. I.; Morone, A.; Salvi, A. M. XPS determination of oxygen-containing functional groups on carbon-fibre surfaces and the cleaning of these surfaces. *Surf. Interface Anal.* **1990**, *15*, 627–634.

(53) Martin, L.; Martinez, H.; Ulldemolins, M.; Pecquenard, B.; Le Cras, F. Evolution of the Si electrode/electrolyte interface in lithium batteries characterized by XPS and AFM techniques: The influence of vinylene carbonate additive. *Solid State Ionics* **2012**, *215*, 36–44.

(54) Mahiudddin, Md.; Fakhruddin, A. N. M.; Abdullah-Al-Mahin. Degradation of phenol via meta cleavage pathway by pseudomonas fluorescens PU1. *ISRN Microbiol.* **2012**, ID741820, http://www.hindawi.com/journals/isrn/2012/741820/

(55) Wang, J.; Fu, W.; He, X.; Yang, S.; Zhu, W. Catalytic wet air oxidation of phenol with functionalized carbon materials as catalysts: Reaction mechanism and pathway. *J. Environ. Sci-China*. **2014**, *26*, 1741–1749.

This is a PDF file of an unedited manuscript that has been accepted for publication. Final edited form is published in *Langmuir, 2014, 30:15451−15461*. http://dx.doi.org/10.1021/la5038102

Supplementary Material to the paper

Mechanism of in-situ surface polymerization of gallic acid in an environmental-inspired preparation of carboxylated core-shell magnetite nanoparticles

Ildikó Y. Tóth, Márta Szekeres, Rodica Turcu, Szilárd Sáringer, Erzsébet Illés, Dániel Nesztor, Etelka Tombácz

Section 1. Results of FITEQL calculation of the pK_a values of GA and GA radicals and relative concentration of GA radicals in the course of acid-base titration

Gallic acid solution in 0.5 M NaCl was titrated with NaOH and subsequently with HCl solutions (up and down titrations, respectively) using the potentiometric method, and the net proton consumption vs pH functions were calculated. We have observed a permanent and time-independent irreversibility between the up and down titrations (Figure S1**)**.

The experimental data were fitted using the program FITEQL [1]. For the up titration, three components attributed to the three protonable moieties of the gallic acid (the carboxylic acid and two types of phenolic OH groups) were used in the equilibrium definition at fixed concentration (i.e., the concentration of the titrated gallic acid solution) and the protonation constants were fitted. The resulting pK_a values pK_{a1}= 4.3, pK_{a2}= 8.8 and pK_{a3}= 11.5 are consistent with the values found for gallic acid in literature [2].

The down titration results were fitted by using five pK_a values: three of them coincide with those in the up titration and two new pK_a's can be assigned to gallic acid radicals formed in the alkaline medium [3, 4]. As the protonation steps attributed to gallate (pK_{a1}= 4.3, pK_{a2}= 8.8) appear clearly in the titration function, it follows that only a partial amount of GA transforms to GA radicals. The data were fitted in FITEQL setting a chemically reasonable model: (i) a mixture of gallic acid and its radical is titrated; (ii) the radical has three types of deprotonated moieties (a carboxylate and two phenolates); (iii) the sum of GA and GA radical concentration is fixed and (iv) the concentrations of the GA radical moieties are fitting parameters. The obtained pK_a* values are pK_{a2}*=6.5 and pK_{a3}*=9.8. 56 % of GA remained in its original form and the concentration of the GA radical moieties assigned to pK_{a2}* and pK_{a3}* is 44 %.

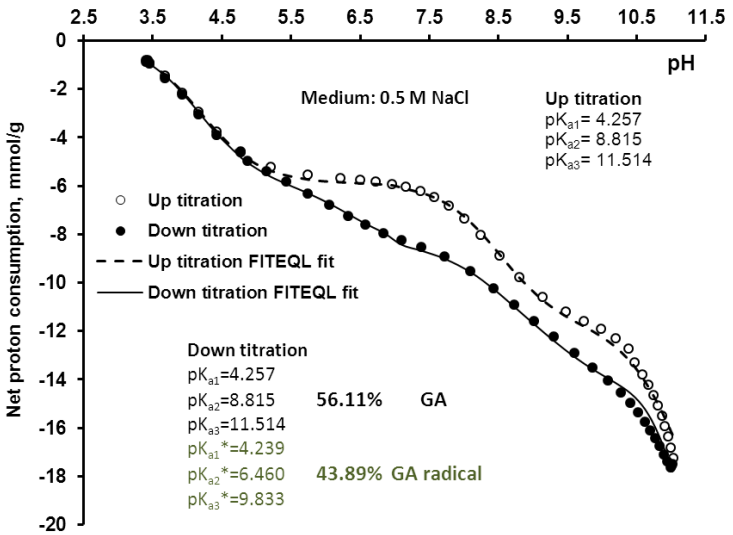

Figure S1. The net proton consumption vs pH functions calculated from the potentiometric acid-base titration of gallic acid. The data were fitted in FITEQL (lines) to determine the pK_a values of GA and its radicals.

References

[1] Westall, J. C.; Herbelin, A. L. FITEQL: a computer program for determination of chemical equilibrium constants from experimental data. (version: 4.0). Oregon State University, Corvallis, Oregon, 1999.

[2] Beltrán, J. L.; Sanli, N.; Fonrodona, G.; Barrón, D.; Özkan, G.; Barbosa, J. Spectrophotometric, potentiometric and chromatographic pK_a values of polyphenolic acids in water and acetonitrile-water media. *Anal. Chim. Acta* **2003**, *484*, 253– 264.

[3] Eslami, A. C.; Pasanphan, W.; Wagner, B. A.; Buettner, G. R. Free radicals produced by the oxidation of gallic acid: An electron paramagnetic resonance study. *Chem. Cent. J.* **2010**, *4*, 15. http://journal.chemistrycentral.com/content/4/1/15 (accessed on 27-11-2014)

[4] Quideau, S.; Deffieux, D.; Douat-Casassus, C.; Pouységu, L. Plant polyphenols: Chemical properties, biological activities, and synthesis. *Angew. Chem., Int. Ed.* **2011**, *50*, 586– 621.

Section 2. Ionic strength effect on the color of GA solutions

The picture below shows the effect of ionic strength on the change of color in GA solutions during the course of down titrations performed in 0.005, 0.05 and 0.5 M NaCl background electrolytes. The photos were taken at pH values 11 and 3. The color change is due to the formation of different GA radicals and dimers/oligomers at high pH in the presence of oxygen.

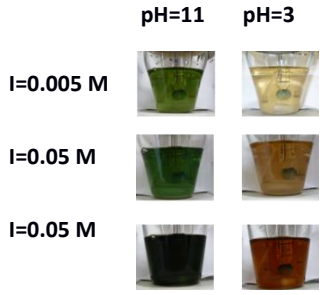

Section 3. Changes in the hydrodynamic diameter of MNPs during polymerization of adsorbed GA

The results of dynamic light scattering determination of hydrodynamic diameters in the course of surface polymerization are demonstrated in the figure below. It is seen that at higher GA loading (10 mmol/g) the size characteristic of polyelectrolyte-coated MNPs (~170 nm) is achieved within two weeks of spontaneous surface induced polymerization of GA while at lower GA loading (0.6 mmol/g), this value is not reached even at the end of the observation period (four weeks). Thus, the thickness of the PGA coating is controlled in principle by both GA loading and time of polymerization.

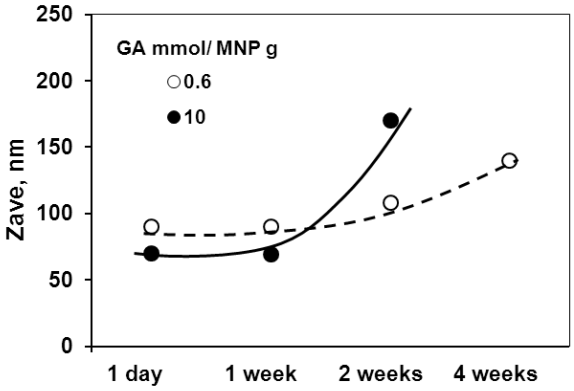

Section 4. TEM analysis of the size distribution of naked and PGA-coated MNPs

TEM images of naked and PGA coated iron oxide nanoparticles were taken in a Philips CM-10 transmission electron microscope supplied with a Megaview-II camera. The accelerating voltage was 100 kV and the maximum resolution of the instrument is ~0.2 nm. The nanoparticles were deposited onto Formwar-coated copper grids from highly diluted dispersions and the medium was removed by the wicking technique. The average size and size distribution were determined by evaluating 100 particles using the JMicrovision 1.2.7. software.

The TEM images are presented in Figure S3. Both the naked and coated MNPs are fairly monodisperse spherical particles with average diameters of 10.5 ± 1.3 nm (inset of the left panel of Figure S3) and 10.3 ± 1.1 nm (inset of the right panel of Figure S3), respectively. The PGA coated nanoparticles are less overlapped compared to the naked ones because the PGA layer acts as a spacer between the magnetic cores.

This is a PDF file of an unedited manuscript that has been accepted for publication. Final edited form is published in *Langmuir, 2014, 30:15451−15461*. http://dx.doi.org/10.1021/la5038102

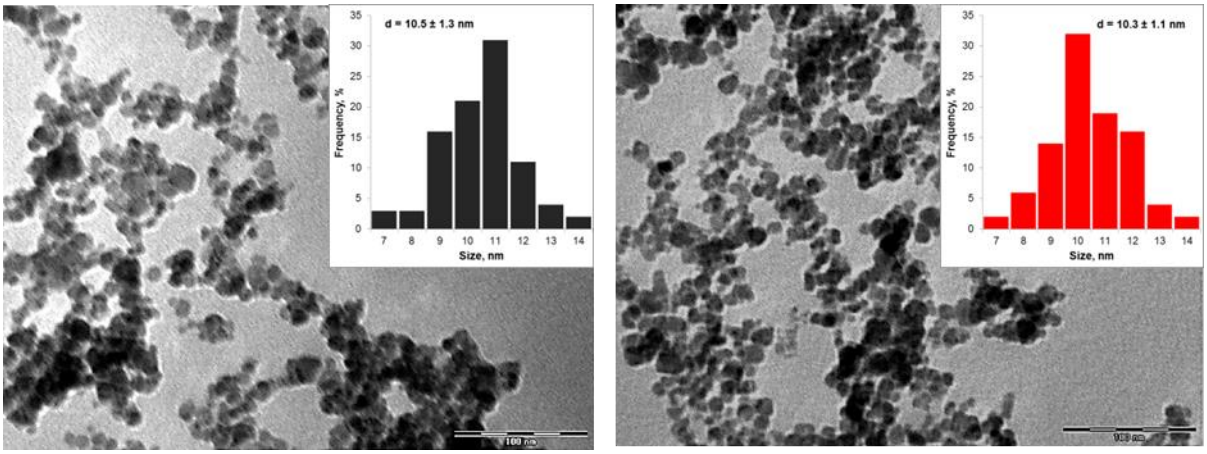

Figure S3. TEM pictures and the size distributions of naked (left) and PGA coated nanoparticles (right) at 130000-fold magnification. The scale bar is 100 nm.

Section 5. Stability of the adsorbed layer of GA molecules on the MNPs

The adsorption and desorption isotherms of GA on MNPs measured at pH~6.5 and 10 mM NaCl are seen below. The arrows indicate the decrease in the GA equilibrium concentration due to dilution of the dispersions. The lines are drawn to guide the eyes. The surface complex formation of two adjacent phenolic groups of GA with one or two surface Fe atoms (bidentate complex or bridging, respectively) of the MNPs is responsible for the dilution stability of the adsorbed layer.

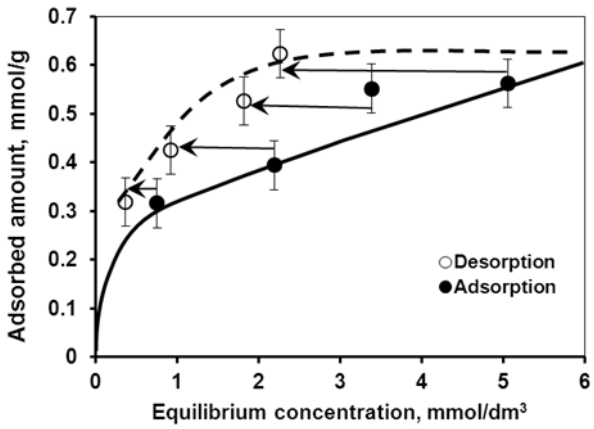

Section 6. pH-dependent aggregation of GA@MNPs and PGA@MNPs as measured by dynamic light scattering.

Above pH ~6, the hydrodynamic diameter (Z_{ave}) of GA coated MNPs (2 mmol GA/g MNP) increased after 4 weeks of preparation due to polymerization of GA in the adsorbed layer. The error bars are omitted for the sake of clarity. The lines are drawn to guide the eyes.

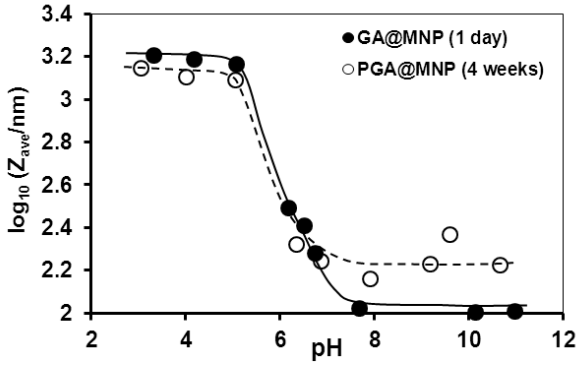

This is a PDF file of an unedited manuscript that has been accepted for publication. Final edited form is published in *Langmuir, 2014, 30:15451−15461*. http://dx.doi.org/10.1021/la5038102

Section 7. Gallate polymerization

The picture below represents the two possible modes of polymerization of GA monomers on the surface of MNPs: ester bridging (A) and ether bridged dimer formation (B). The C–O bridged dimers (B) were identified by Oniki and Takahama in solution phase (*J. Wood Sci.* **2004**, *50*, 545–547, reference [39] in the manuscript).